A Three-Time-Level Explicit Economical (3TL-EEC) Time-Difference Scheme

Sajal K. Kar[1,2] and Zavisa Janjic[2]

[1]I. M. Systems Group, Inc., Rockville, MD

[2]NOAA/NWS/NCEP/EMC, Camp Springs, MD

February 2012

Corresponding author address: Dr. Sajal K. Kar, W/NP2 RM 207, WWBG

5200 Auth Road, Camp Springs, MD 20746-4304

E-mail: Sajal.Kar@noaa.gov

ABSTRACT

A new three-time-level explicit economical scheme (acronym 3TL-EEC) has been proposed that allows a stable time step for gravity-wave propagation that is twice as large as the stable time step permitted by the standard three-time-level leapfrog scheme. In a two-time-level frame-work, the well-established and widely-used forward-backward scheme is already known to allow a stable time step for gravity-wave propagation that is twice the time step allowed by the leapfrog scheme. However, when the forward-backward scheme is applied over two time steps (say, from the time-level n-1 to n+1) of the leapfrog scheme, the computational economy of the forward-backward scheme over the leapfrog scheme is lost. Thus, there is no benefit in computational efficiency if the forward-backward scheme is applied for the gravity waves in combination with the leapfrog scheme, e.g., for the advection and Coriolis terms. The proposed 3TL-EEC scheme was derived from the forward-backward scheme using an original and innovative approach. The new scheme recaptures the latter scheme's attractive features of computational economy in a three-time-level frame-work, and thereby allows for the use of the leapfrog scheme for advection and Coriolis effects. Detailed stability properties of the 3TL-EEC scheme will be presented for the 1D shallow-water (pure) gravity waves and 2D shallow-water gravity waves on an f-plane with uniform advection; and compared with the corresponding properties of the leapfrog scheme. The 3TL-EEC scheme, in conjunction with the leapfrog scheme for advection and Coriolis effects, has been implemented in a global grid-point shallow-water model that conserves potential enstrophy and total energy on the Arakawa C grid. Lastly, the numerical accuracy and stability of the proposed scheme will be demonstrated and compared to the same aspects

of the leapfrog scheme, via numerical time integrations of the aforementioned global shallow-water model, starting with the Rossby-Haurwitz wave number 4 initial conditions.

1. Introduction

The forward-backward (FB) scheme is a 2-time-level scheme that allows a stable time step twice that of the standard 3-time-level leapfrog (LF) scheme for the gravity-wave propagation. Since the FB scheme is a 2-time-level scheme, it has been convenient to use another 2-time-level scheme such as the non-split Adams-Bashforth (AB) scheme for the advection, as currently done in the NCEP unified Nonhydrostatic Multiscale Model on the Arakawa B grid (NMMB) or to use an iterative 2-time-level scheme with or without splitting at a higher cost penalty. For details of the NMMB, the reader is referred to Janjic (2010) and the references therein.

Potential use of the LF scheme in place of the AB scheme for advection in NMMB, without losing the computational economy of the FB scheme for the gravity-wave propagation, is our motivation behind this research. Following Janjic's idea, we have developed a new 3-time-level explicit economical (3TL-EEC) scheme that retains the computational economy of the FB scheme, and enables use of the LF scheme for advection. This scheme is potentially useful for improving the numerical accuracy and efficiency of the NMMB.

In section 2, we present the mathematical formulation of the 3TL-EEC scheme, starting with a review of the standard leapfrog (LF) scheme and the forward-backward (FB) scheme in case of the 1D shallow-water (pure) gravity waves without rotation and advection. Then, the 3TL-EEC scheme and the 3TL-EEC_LF schemes are introduced in terms of the 1D shallow-water waves and later applied to the 2D shallow-water gravity waves on a *f*-plane including uniform advecion. Detailed von Neumann stability analyses of the 3TL-EEC and 3TL-EEC+LF schemes are carried out in the framework of the linear shallow-water equations. Lastly, the LF and 3TL-EEC+LF schemes are implemented in a global, grid-point, nonlinear shallow-water model and time integrations are performed for 210 days, starting with the Rossby-Haurwitz zonal wavenumber 4 initial condition. A brief summary is presented in section 3.

2. The three-time-level explicit economical scheme

a. Formulation of the scheme

To review the FB and LF schemes, and later introduce the 3TL-EEC scheme, we employ the 1D shallow-water gravity-wave equations:

$$\partial_t \eta + c\partial_x u = 0, \tag{2.1a}$$
$$\partial_t u + c\partial_x \eta = 0, \tag{2.1b}$$

where $\eta(x,t) = \sqrt{g/H}\,h(x,t)$ and $c \equiv \sqrt{gH}$ denotes the phase speed of the gravity waves. Here H is the constant height of the free surface for the basic state; h is the deviation of the height from H for a perturbed state; and u is the perturbation velocity in the x-positive direction.

1) Review of the Leapfrog scheme

Let $n-1$, n, and $n+1$ denote the indices of the three time levels involved and Δt denotes the time step. The leapfrog (LF) scheme for the 1D shallow-water gravity-wave equations (2.1a) and (2.1b) is given by

$$\frac{\eta^{n+1}-\eta^{n-1}}{2\Delta t}+c\partial_x u^n=0\,, \tag{2.2a}$$

$$\frac{u^{n+1}-u^{n-1}}{2\Delta t}+c\partial_x \eta^n=0\,. \tag{2.2b}$$

For a traditional von Neumann stability analysis of the LF scheme, we assume solutions for (2.2a) and (2.2b) in the form

$$(u,\eta)^n=\mathrm{Re}[\lambda^n(u_0,\eta_0)e^{ikx}]\,, \tag{2.3}$$

where λ is the (complex) amplification factor and k is the wavenumber in *x*. The amplification factor (λ) for the LF scheme [(2.2a) and (2.2b)] satisfies a biquadratic equation

$$(\lambda^2-1)^2+4p^2\lambda^2=0\,, \tag{2.4}$$

where $p\equiv kc\Delta t$. For (2.4), there are two physical (gravity-wave) modes and two computational modes in time. All modes are stable and neutral. For stability, $|p|\le 1$.

2) Review of the forward-backward scheme

Forward step for (2.1a)

$$\frac{\eta^{n+1}-\eta^{n}}{\Delta t}+c\partial_x u^n=0\,, \tag{2.5a}$$

Backward step for (2.1b)

$$\frac{u^{n+1}-u^{n}}{\Delta t}+c\partial_{x}\eta^{n+1}=0\,. \qquad (2.5b)$$

The amplification factor (λ) for the forward-backward (FB) scheme [(2.5a) and (2.5b)] satisfies a quadratic equation

$$\lambda^2+(p^2-2)\lambda+1=0\,. \qquad (2.6)$$

In (2.6), there are two physical (gravity-wave) modes, but no computational mode in time. For stability, $|p|\le 2$. Since the FB scheme requires $|p|\le 2$ compared to $|p|\le 1$ for the LF scheme, the FB scheme is clearly economical with a stable time step twice as large as the LF scheme.

3) THE THREE-TIME-LEVEL EXPLICIT ECONOMICAL SCHEME

As suggested by Janjic, to construct the 3TL-EEC scheme for the 1D gravity-wave system, we first apply the FB scheme from time-level *n*-1 to *n*:

$$\frac{\eta^{n}-\eta^{n-1}}{\Delta t}+c\partial_{x}u^{n-1}=0\,, \qquad (2.7a)$$

$$\frac{u^{n}-u^{n-1}}{\Delta t}+c\partial_{x}\eta^{n}=0\,. \qquad (2.7b)$$

Then, we reapply the FB scheme from time-level *n* to *n*+1:

$$\frac{\eta^{n+1}-\eta^{n}}{\Delta t}+c\partial_{x}u^{n}=0\,, \qquad (2.8a)$$

$$\frac{u^{n+1}-u^{n}}{\Delta t}+c\partial_{x}\eta^{n+1}=0\,. \qquad (2.8b)$$

Lastly, we take an average of the respective equations above [i.e., (2.7a+2.8a)/2 and (2.7b+2.8b)/2] to introduce the **3TL-EEC scheme**:

$$\frac{\eta^{n+1}-\eta^{n-1}}{2\Delta t}+\frac{c}{2}\partial_x(u^n+u^{n-1})=0, \tag{2.9a}$$

$$\frac{u^{n+1}-u^{n-1}}{2\Delta t}+\frac{c}{2}\partial_x(\eta^{n+1}+\eta^n)=0. \tag{2.9b}$$

The amplification-factor (λ) for the 3TL-EEC scheme [(2.9a) and (2.9b)] satisfies the quadratic equations

$$(\lambda+1)^2=0, \tag{2.10a}$$

$$\lambda^2+(p^2-2)\lambda+1=0. \tag{2.10b}$$

Equation (2.10b) is identically same as (2.6) for the FB scheme. Thus, **the 3TL-EEC scheme maintains the favorable economy and stability properties of the FB scheme**. While (2.10a) shows that unlike the FB scheme, the 3TL-EEC scheme introduces two computational modes; but like the LF scheme, these modes are neutrally stable.

4) A Combination of the 3TL-EEC and LF Schemes

Including a uniform advection-velocity of U in the x-direction, the 1D shallow water equations (2.1a) and (2.1b) can be rewritten as

$$\partial_t\eta+c\partial_x u+U\partial_x\eta=0, \tag{2.11a}$$

$$\partial_t u+c\partial_x\eta+U\partial_x u=0. \tag{2.11b}$$

Let us now design a three-time-level scheme for (2.11a) and (2.11b), in which the 3TL-EEC scheme is used for the gravity-wave terms (i.e., $c\partial_x u$ and $c\partial_x\eta$) and the LF scheme is used for the advection terms (i.e., $U\partial_x\eta$ and $U\partial_x u$). This combination (termed as 3TL-EEC+LF) scheme can be expressed as

$$\frac{\eta^{n+1}-\eta^{n-1}}{2\Delta t}+\frac{c}{2}\partial_x(u^n+u^{n-1})+U\partial_x\eta^n=0, \tag{2.12a}$$

$$\frac{u^{n+1}-u^{n-1}}{2\Delta t}+\frac{c}{2}\partial_x(\eta^{n+1}+\eta^n)+U\partial_x u^n=0. \tag{2.12b}$$

For a von Neumann stability analysis of the 3TL-EEC+LF scheme [(2.12a) and (2.12b)], we assume normal-mode solutions of the form

$$u(x,t^n)=\mathrm{Re}(u_0\lambda^n e^{ikx});\ \eta(x,t^n)=\mathrm{Re}(\eta_0\lambda^n e^{ikx}), \tag{2.13}$$

where λ is the (complex) amplification factor, (u_0, η_0) are the wave (complex) amplitudes at initial time, and $i\equiv\sqrt{-1}$ is the imaginary unity. Substituting (2.13) in (2.12a) and (2.12b), and then solving for nonzero values of u_0 and η_0, we derive a biquadratic equation for λ given by

$$\lambda^4+(p^2+i4q)\lambda^3+(2p^2-2-4q^2)\lambda^2+(p^2-i4q)\lambda+1=0, \tag{2.14}$$

where $p\equiv kc\Delta t$ (as before) and $q\equiv kU\Delta t$. Because of the complex coefficients in (2.14), we have not attempted to solve it analytically. For the numerical solutions of (2.14), (i) we have varied p over the range of $|p|\le 2$, so that the 3TL-EEC part of the 3TL-EEC+LF scheme can be stable for the gravity-wave terms; and (ii) we have varied q over the range of $|q|\le 1$, so that the LF part of the 3TL-EEC+LF scheme can be stable for the advection terms. Let λ_j, with $j=1$, 2, 3, and 4, denote the four roots of (2.14). Then, the 3TL-EEC+LF scheme is considered to be (a) stable when $|\lambda_j|<1-\varepsilon$; (b) neutral when $1-\varepsilon<|\lambda_j|<1+\varepsilon$; and (c) unstable when $|\lambda_j|>1+\varepsilon$, where each stability criterion is required to be satisfied for all *j*. Specifically, for $\varepsilon=1.\times10^{-8}$ and ($0\le p\le 2$, $0\le q\le 1$), we have solved (2.14) in double precision for $\lambda_j(p,q)$ and then plotted the function

$\Lambda \equiv \max_j |\lambda_j(p, q)|$ in Fig. 1. The region of neutral stability with $\Lambda \cong 1$ falls below the contour labeled 1, and is approximately satisfied by the inequality $p/1.7 + q/0.9 \le 1$.

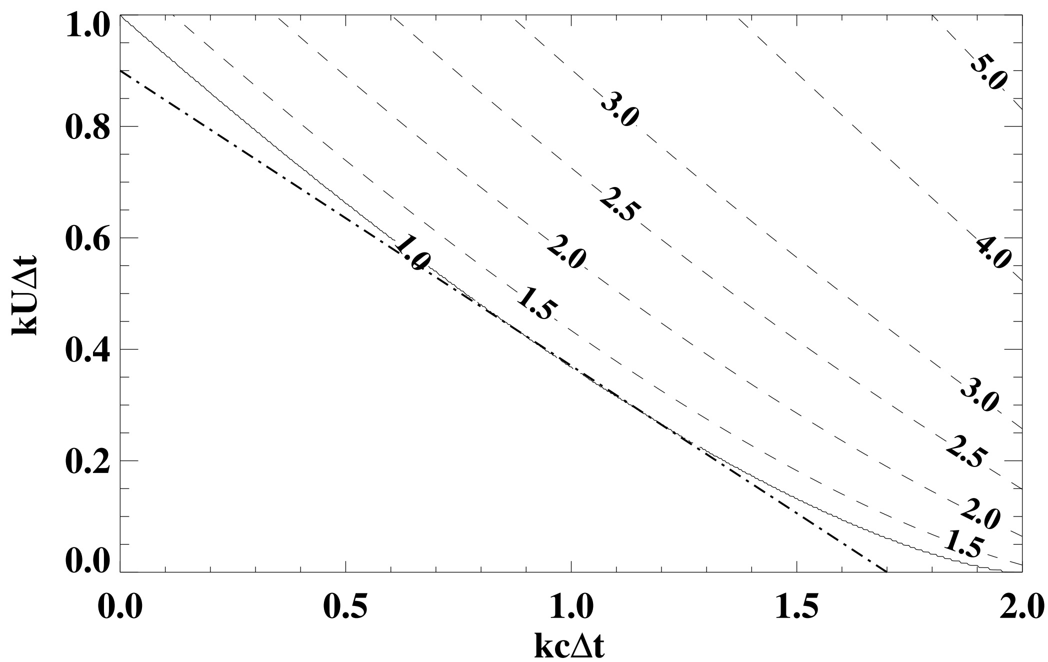

Fig. 1. Contours of the maximum value (Λ) from the absolute magnitudes of the four roots of the equation (2.14), which governs the amplification factor (λ) for the 3TL-EEC+LF scheme applied to the 1D shallow-water equation including uniform advection. The abscissa and ordinate are given by $p \equiv kc\Delta t$ and $q \equiv kU\Delta t$, respectively. The 3TL-EEC+LF scheme is neutrally stable in the region below the unity contour line. The dashed contours fall inside the unstable region. The dash-dotted straight line, $p/1.7 + q/0.9 = 1$, has been drawn so that the neutral stability region is approximately determined by the inequality $p/1.7 + q/0.9 \le 1$.

5) Stability analysis of the 3TL-EEC+LF and the LF schemes applied to the 2D shallow-water gravity-inertia wave equations

Here, we consider the 2D shallow-water gravity-inertia waves on a *f*-plane in Cartesian geometry, including uniform advection with the velocity components *U* in *x* and V in y. On a staggered Arakawa C grid, the governing equations are written in a form that is continuous in time, but center-differenced in x and y, as follows:

$$\partial_t \eta + U\overline{\delta_x \eta}^x + V\overline{\delta_y \eta}^y + c(\delta_x u + \delta_y v) = 0, \tag{2.15a}$$

$$\partial_t u + U\overline{\delta_x u}^x + V\overline{\delta_y u}^y - f\overline{v}^{xy} + c\delta_x \eta = 0, \tag{2.15b}$$

$$\partial_t v + U\overline{\delta_x v}^x + V\overline{\delta_y v}^y + f\overline{u}^{xy} + c\delta_y \eta = 0, \tag{2.15c}$$

where the subscript denotes a second-order centered-difference operator in x or y, and the superscript denotes an averaging operator in x and/or y. Both operators are applied over a uniform grid interval d. Here, $c \equiv \sqrt{gH}$ (as before), and $\eta(x, y, t) \equiv \sqrt{g/H}\, h(x, y, t)$.

Assuming normal-mode solutions of equations (2.15) in the form:

$$\psi_{i,j}(t) = \mathrm{Re}[\hat{\psi}(t)\exp\{\hat{i}(ikd + jld)\}], \tag{2.16}$$

where $\hat{i} \equiv \sqrt{-1}$; and i and j denote the grid-indices in x and y, respectively. Also, k and l denote the wavenumbers in x and y, respectively. Substituting (2.16) in (2.15) and rewriting the equations we obtain

$$\Delta t(d_t \hat{\eta}) + \hat{i}A\hat{\eta} + \hat{i}(K\hat{u} + L\hat{v}) = 0, \tag{2.17a}$$

$$\Delta t(d_t \hat{u}) + \hat{i}A\hat{u} - F\hat{v} + \hat{i}K\hat{\eta} = 0, \tag{2.17b}$$

$$\Delta t(d_t \hat{v}) + \hat{i}A\hat{v} + F\hat{u} + \hat{i}L\hat{\eta} = 0, \tag{2.17c}$$

where the non-dimensional parameters A, F, K, and L are defined by

$$A \equiv \frac{U\Delta t}{d}\sin kd + \frac{V\Delta t}{d}\sin ld, \tag{2.18a}$$

$$F \equiv (f\Delta t)\cos\frac{kd}{2}\cos\frac{ld}{2}, \tag{2.18b}$$

$$K \equiv \frac{2c\Delta t}{d}\sin\frac{kd}{2}\,, \tag{2.18c}$$

$$L \equiv \frac{2c\Delta t}{d}\sin\frac{ld}{2}\,. \tag{2.18d}$$

Following subsection 2a.4, the 3TL-EEC+LF scheme for the equations (2.17) can be written as

$$\tfrac{1}{2}(\hat{\eta}^{n+1} - \hat{\eta}^{n-1}) + \hat{i}A\hat{\eta}^{n} + \tfrac{1}{2}\hat{i}[K(\hat{u}^{n} + \hat{u}^{n-1}) + L(\hat{v}^{n} + \hat{v}^{n-1})] = 0\,, \tag{2.19a}$$

$$\tfrac{1}{2}(\hat{u}^{n+1} - \hat{u}^{n-1}) + \hat{i}A\hat{u}^{n} - F\hat{v}^{n} + \tfrac{1}{2}\hat{i}K(\hat{\eta}^{n} + \hat{\eta}^{n+1}) = 0\,, \tag{2.19b}$$

$$\tfrac{1}{2}(\hat{v}^{n+1} - \hat{v}^{n-1}) + \hat{i}A\hat{v}^{n} + F\hat{u}^{n} + \tfrac{1}{2}\hat{i}L(\hat{\eta}^{n} + \hat{\eta}^{n+1}) = 0\,. \tag{2.19c}$$

Then, for a von Neumann stability analysis of the 3TL-EEC+LF scheme (2.19), we further substitute

$$\hat{\psi}^{n} = \psi_0\lambda^{n}\,, \tag{2.20}$$

for $\hat{u}$, $\hat{v}$, and $\hat{\eta}$ in (2.19), and for a nontrivial solution of u_0, v_0, and η_0, obtain the governing equations for the (complex) amplification factor λ in (2.20) as

$$\tfrac{1}{2}(\lambda^2 - 1) + \hat{i}A\lambda = 0\,, \tag{2.21a}$$

$$\left\{\tfrac{1}{2}(\lambda^2 - 1) + \hat{i}A\lambda\right\}^2 + (F\lambda)^2 + \tfrac{1}{4}(K^2 + L^2)\lambda(\lambda + 1)^2 = 0\,. \tag{2.21b}$$

Here (2.21a) corresponds to the stationary geostrophic wave modes in time (one physical and the other computational), and (2.21b) corresponds to the transient gravity-inertia wave modes in time (two physical and the other two computational).

Similarly, the LF scheme for the equations in (2.17) can be written as

$$\tfrac{1}{2}(\hat{\eta}^{n+1} - \hat{\eta}^{n-1}) + \hat{i}A\hat{\eta}^{n} + \hat{i}(K\hat{u}^{n} + L\hat{v}^{n}) = 0\,, \tag{2.22a}$$

$$\tfrac{1}{2}(\hat{u}^{n+1} - \hat{u}^{n-1}) + \hat{i}A\hat{u}^{n} - F\hat{v}^{n} + \hat{i}K\hat{\eta}^{n} = 0\,, \tag{2.22b}$$

$$\tfrac{1}{2}(\hat{v}^{n+1} - \hat{v}^{n-1}) + \hat{i}A\hat{v}^n + F\hat{u}^n + \hat{i}L\hat{\eta}^n = 0\,. \tag{2.22c}$$

The amplification factor (λ) for the LF scheme (above), satisfies the same equation (2.21a) for the stationary geostrophic wave modes, but for the transient gravity-inertia wave modes, (2.21b) is replaced by

$$\left\{\tfrac{1}{2}(\lambda^2 - 1) + \hat{i}A\lambda\right\}^2 + (F^2 + K^2 + L^2)\lambda^2 = 0\,. \tag{2.23}$$

In the following discussion, we focus only on the stability of the transient gravity-inertia modes for the 3TL-EEC+LF and the LF schemes. For the particular case of the (pure) gravity waves with no advection ($U = V = 0$) and no rotation ($f = 0$), equation (2.21b) for the 3TL-EEC+LF scheme (or, effectively for the 3TL-EEC scheme) can be reduced to the equations

$$(\lambda + 1)^2 = 0\,, \tag{2.24a}$$

$$\lambda^2 + (K^2 + L^2 - 2)\lambda + 1 = 0\,. \tag{2.24b}$$

Here (2.24a) and (2.24b) are analogous with (2.10a) and (2.10b), respectively. For stability of the 3TL-EEC+LF scheme in (2.24b), one requires

$$\sqrt{K^2 + L^2} \le 2\,, \text{ or, } \frac{c\Delta t}{d}\left[\sin^2\frac{kd}{2} + \sin^2\frac{ld}{2}\right]^{1/2} \le 1\,,$$

for all kd and ld values in the ranges $0 \le kd \le \pi$ and $0 \le ld \le \pi$. Thus, **the stability inequality for the 3TL-EEC+LF scheme** is finally reduced to

$$\frac{c\Delta t}{d} \le \frac{1}{\sqrt{2}} \cong 0.707\,. \tag{2.25}$$

Similarly, using (2.23) with no advection ($U = V = 0$) and no rotation ($f = 0$), **the stability inequality for the LF scheme** can be derived as

$$\frac{c\Delta t}{d} \le \frac{1}{2\sqrt{2}} \cong 0.35 \,. \tag{2.26}$$

In (2.25) and (2.26), the ratio $c\Delta t/d$ can be identified as the (pure) gravity-wave Courant number, $\mu_g \equiv c\Delta t/d$, for the space- and time-discretized systems (2.19) and (2.22). We notice that the computational economy of the 3TL-EEC scheme over the LF scheme is maintained (not surprisingly) for the 2D shallow-water (pure) gravity waves.

For the general case of the gravity-inertia waves with advection, the equation (2.21b) for the 3TL-EEC+LF scheme and (2.23) for the LF scheme, need to be solved numerically to determine the amplification factor λ. Equations (2.21b) and (2.23) are expanded to derive the following biquadratic equations in λ:

$$\lambda^4 + (B + \hat{i}4A)\lambda^3 + \{4(F^2 - A^2) + 2(B-1)\}\lambda^2 + (B - \hat{i}4A)\lambda + 1 = 0 \,, \tag{2.27a}$$

$$\lambda^4 + \hat{i}4A\lambda^3 + \{4(F^2 - A^2) + 2(2B-1)\}\lambda^2 - \hat{i}4A\lambda + 1 = 0 \,, \tag{2.27b}$$

where $B \equiv K^2 + L^2$, with *A*, *F*, *K*, and *L* are as defined in (2.18). For numerical solutions of (2.27a) and (2.27b), we set the parameters as follows:

$$\left.\begin{array}{c} f = 10^{-4}\ \text{s}^{-1} \\ c = 100\,\text{ms}^{-1}; \quad U = V = 100/\sqrt{2}\ \text{ms}^{-1} \\ d = 500\ \text{km}, 100\ \text{km} \\ 0 \le \text{kd} \le \pi, \quad 0 \le \text{ld} \le \pi \\ \text{3TL-EEC+LF scheme}: (c + \sqrt{U^2 + V^2})\Delta t/d \le 0.7 \\ \text{LF scheme}: (c + \sqrt{U^2 + V^2})\Delta t/d \le 0.35 \end{array}\right\} . \tag{2.28}$$

The stability inequalities for the two schemes as specified in (2.28) are not analytically derived, but are approximate logical extensions of the inequalities in (2.25) and (2.26), in which the pure gravity-wave speed *c* has been augmented by the 2D advection wind-speed $\sqrt{U^2 + V^2}$. For solving (2.27), we specify a value of the Courant number

$\mu \equiv (c+\sqrt{U^2+V^2})\Delta t/d$, and compute the time step as $\Delta t = \mu d/(c+\sqrt{U^2+V^2})$. Then, biquadratic equations in (2.27) are solved in double precision using the IDL subroutine FZ_ROOTS. We have computed the roots of (2.27a) for the 3TL-EEC+LF scheme, for $\mu \le 0.7$ and $\mu = 0.71$, and found the scheme is unstable for $\mu = 0.71$, but neutrally stable for $\mu \le 0.7$. Specifically, for $\mu \le 0.7$, $|\lambda_j| \cong 1$ for *j* = 1, 2, 3, and 4. Similarly, we have computed the roots of (2.27b) for the LF scheme, for $\mu \le 0.35$ and $\mu = 0.45$. The LF scheme is unstable for $\mu = 0.45$, but neutrally stable for $\mu \le 0.35$. Thus, the 3TL-EEC+LF scheme provides a neutrally-stable time step that is twice that of the standard LF scheme.

To display the stability properties of the two schemes, we have computed the maximum value (Λ) from the absolute values of the four roots of (2.27a) in case of the 3TL-EEC+LF scheme and (2.27b) in case of the LF scheme. Specifically, Λ is defined by

$$\Lambda \equiv \max_j \left|\lambda_j(kd, ld)\right|, \quad j = 1, 2, 3, 4. \tag{2.29}$$

For $d = 100$ km, Fig. 2 shows the surface plots of Λ for the LF scheme using $\mu = 0.45$ and $\mu = 0.35$. For the same value of *d*, Fig. 3 shows the surface plots of Λ for the 3TL-EEC+LF scheme using $\mu = 0.71$ and $\mu = 0.7$. These two figures clearly show that the LF and the 3TL-EEC+LF schemes are (a) neutrally stable for $\mu = 0.35$ and $\mu = 0.7$, respectively, and (b) unstable for $\mu = 0.71$ and $\mu = 0.45$, respectively.

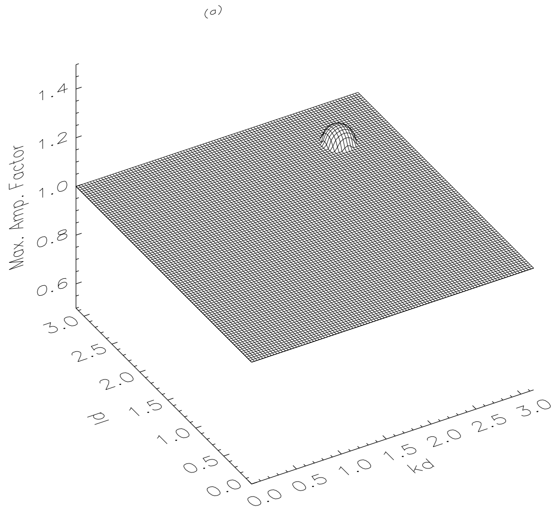

Fig. 2. LF scheme: surface plot of the maximum value (Λ) from the absolute magnitudes of the four roots of the equation (2.27b) for (a) $\mu = 0.45$ and (b) $\mu = 0.35$. The abscissa and ordinate are given by kd and ld, respectively. The grid size, $d = 100\,\mathrm{km}$. The (*U*, *V*) vector is at an angle of 45º with the abscissa. The bump in panel (a) indicates the wavenumber location where the LF scheme becomes unstable for $\mu = 0.45$.

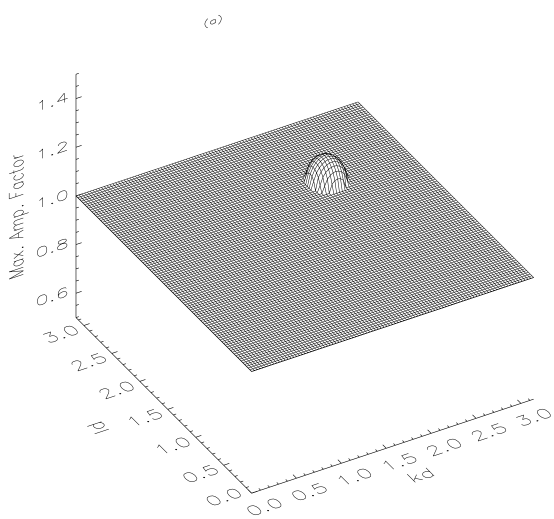

Fig. 3. 3TL-EEC+LF scheme: surface plot of the maximum value (Λ) from the absolute magnitudes of the four roots of the equation (2.27a) for (a) $\mu = 0.71$ and (b) $\mu = 0.7$. The abscissa and ordinate are given by kd and ld, respectively. The grid size, $d = 100\,\mathrm{km}$. The bump in panel (a) indicates the wavenumber location where the 3TL-EEC+LF scheme becomes unstable for $\mu = 0.71$.

b. Application of the 3TL-EEC+LF scheme in a global shallow-water model

To test the effectiveness of the 3TL-EEC+LF scheme in a numerical model that bears a conceptual connection with complex three-dimensional atmospheric and oceanic numerical models, we have implemented the proposed time-difference scheme in a global, grid-point, nonlinear, shallow-water model (Kar et al. 1994, hereafter K94). The 3TL-EEC+LF scheme for the shallow-water model can be expressed as

$$\frac{\Delta\xi\Delta\eta}{mn}\frac{\phi^{n+1}-\phi^{n-1}}{2\Delta t}+\frac{\Phi_0}{2}\left\{\frac{\Delta\eta}{n}\delta_\xi(u^n+u^{n-1})+\delta_\eta\left[(v^n+v^{n-1})\frac{\Delta\xi}{m}\right]\right\}=\tilde{C}^n, \tag{2.30a}$$

$$\frac{\Delta\xi}{m}\frac{u^{n+1}-u^{n-1}}{2\Delta t}+\frac{1}{2}\delta_\xi(\phi^{n+1}+\phi^n)=\tilde{A}^n, \tag{2.30b}$$

$$\frac{\Delta\eta}{n}\frac{v^{n+1}-v^{n-1}}{2\Delta t}+\frac{1}{2}\delta_\eta(\phi^{n+1}+\phi^n)=\tilde{B}^n, \tag{2.30c}$$

where the details of the notations used in the equations above, can be found in K94. The corresponding LF scheme used in the shallow-water model is given by the equations (2.14), (2.15), and (2.16) in K94. In addition, to suppress the separation of the numerical solutions at even and odd time steps, a time filter (Robert 1966; Asselin 1972) is used in the model for the LF and 3TL-EEC+LF time integrations. For an arbitrary prognostic field ψ, the Rober-Asselin time-filter is defined by

$$\overline{\psi}^n=\psi^n+\frac{\nu}{2}(\psi^{n+1}-2\psi^n+\overline{\psi}^{n-1}), \tag{2.31}$$

where ν is the filter parameter and the overbar denotes a time-filtered quantity.

In this global, grid-point, shallow-water model, the horizontal finite-difference scheme is based on the second-order mass-conserving and partial fourth-order energy and potential-enstrophy conserving scheme on the staggered C grid (Arakawa and Lamb

1981). A zonal polar filter is employed at the high latitudes so that a reasonably large time step can be used without violating the CFL stability restriction on time steps arising due to the progressively reduced zonal grid intervals near the poles. Details regarding the finite-differencing and the zonal polar filter used in the shallow-water model can be found in K94.

We have carried out a numerical time integration of the global shallow-water model using the Rossby-Haurwitz wave initial condition. The non-divergent Rossby-Harurwitz (hereafter R-H) wave initial condition, originally introduced by Phillips (1959), has been adopted by Williamson et al. (1992) in a test suite designed specifically for testing newly-developed schemes for the global shallow water models.

The constant parameters related to the R-H wave are the zonal wavenumber, $s = 4$, $\omega = K = 7.848 \times 10^{-6}\,\mathrm{s}^{-1}$, and the initial depth of the shallow water at the poles, $h_0 = 8 \times 10^3\,\mathrm{m}$. In the non-divergent, barotropic continuum, the R-H zonal wavenumber 4 pattern is analytically determined to move from west to east, without a change of shape, at an approximate angular velocity of $12.19^\circ\,\mathrm{day}^{-1}$. Above choice of the parameters ω and K leads to an initial zonal wind maximum of $99\ \mathrm{ms}^{-1}$ and an initial latitudinal wind maximum of $65\ \mathrm{ms}^{-1}$. Assuming the mean depth of the shallow water as h_0, the free-surface gravity-wave speed on the sphere is approximated as $\sqrt{gh_0} \approx 280.09\ \mathrm{m\,s}^{-1}$.

For the numerical time integrations, the shallow-water model is configured with a uniform latitude-longitude grid resolution of $\Delta\varphi = 4^\circ$ and $\Delta\lambda = 5^\circ$. The zonal grid interval centered at the free-surface height (h) points of the C grid ranges from a value of

555.98 km near the equator to 38.80 km near the poles. The latitudinal grid interval, on the other hand, takes on a uniform value of 444.5 km over the entire sphere.

The shallow-water model has been integrated in time for 210 days, first using the LF scheme and then using the 3TL-EEC+LF scheme. The time steps used for the LF and the 3TL-EEC+LF scheme are 40 s and 80 s, respectively, without the polar filter; and 240 s and 480 s, respectively, with the polar filter. For the Robert-Asselin time-filter applied in both schemes, a common value of $\nu = 0.125$ is used.

Figure 3 shows the initial free-surface height on a north polar stereographic projection, clearly depicting a R-H wavenumber 4 pattern. For time integrations performed *without* the polar filter, Fig. 4 shows the height fields predicted by the time-filtered LF and 3TL-EEC+LF schemes on day 15, day 30, and day 60. Similarly, for time integrations performed *with* the polar filter, Fig. 5 shows the height fields on day 15, day 30, and day 60, predicted by the two schemes. On a subjective visual comparison, the height fields predicted by the time-filtered 3TL-EEC+LF scheme seem just as stable and accurate as those produced by the time-filtered LF scheme. Since the time-filtered 3TL-EEC+LF scheme, with or without the polar filter, employs a stable time step that is twice as large as that the stable time step employed by the time-filtered LF scheme, the computational economy associated with the proposed scheme has been firmly established by the shallow-water model solutions presented here.

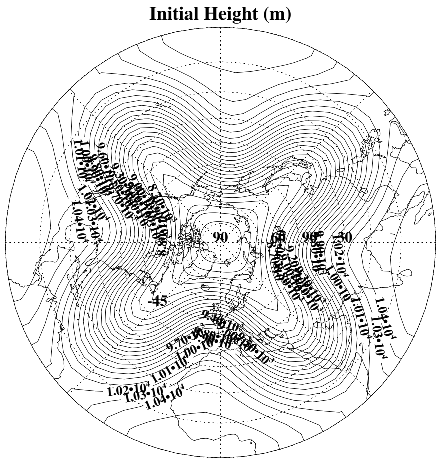

Fig. 3. Initial field of the free-surface height (m) on a north polar-stereographic projection, for the Rossby-Haurwitz zonal wavenumber 4. The contour interval is 100 m.

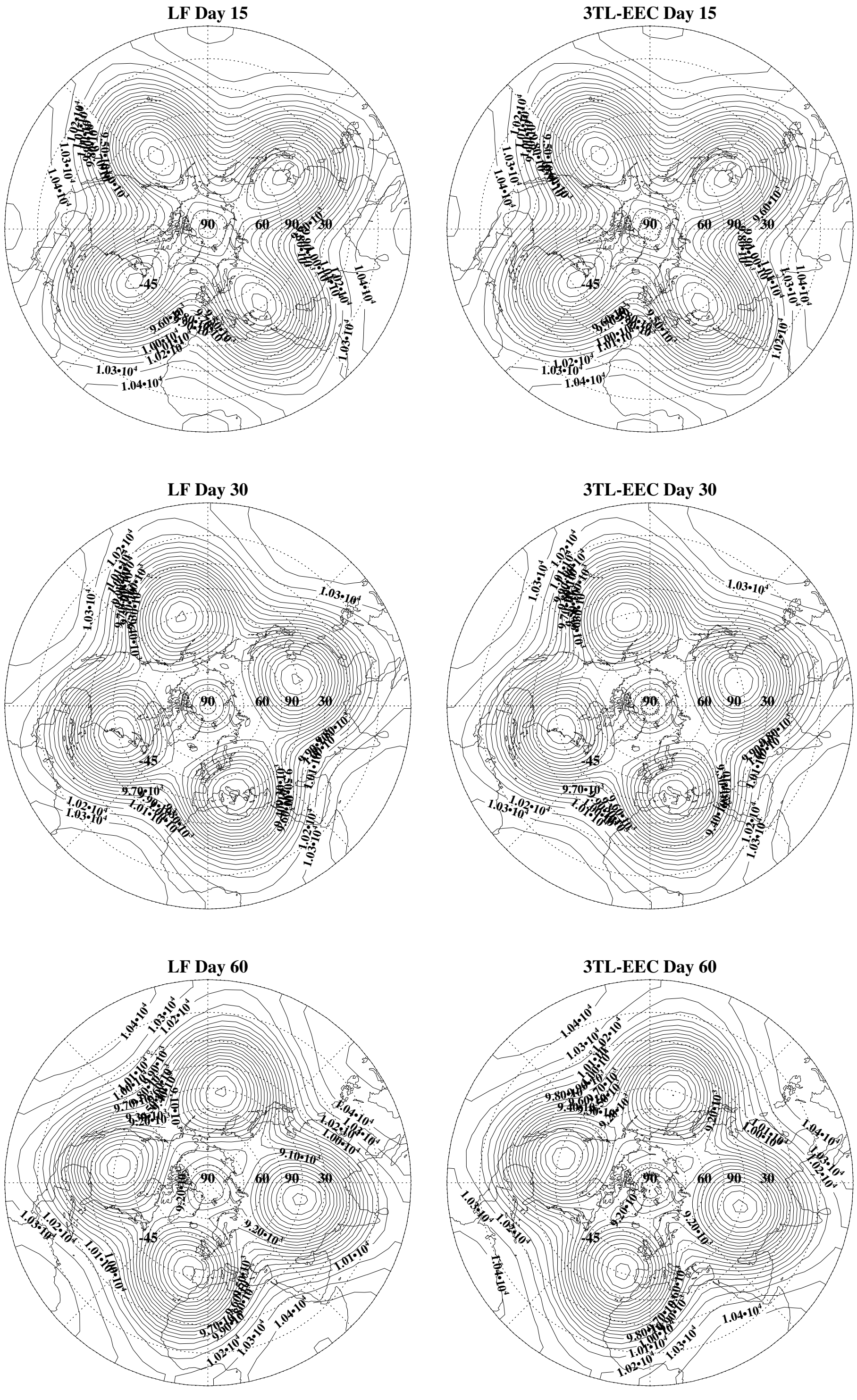

Fig. 4. Free-surface height field (m) predicted by the global shallow-water model using the time-filtered LF scheme, on left column, on day 15 (top), day 30 (middle), and day 60 (bottom). The corresponding forecasts for the time-filtered 3TL-EEC+LF scheme are shown in the right column. There is no polar filter, and the time step used by the LF and 3TL-EEC scheme are 40 s and 80 s, respectively.

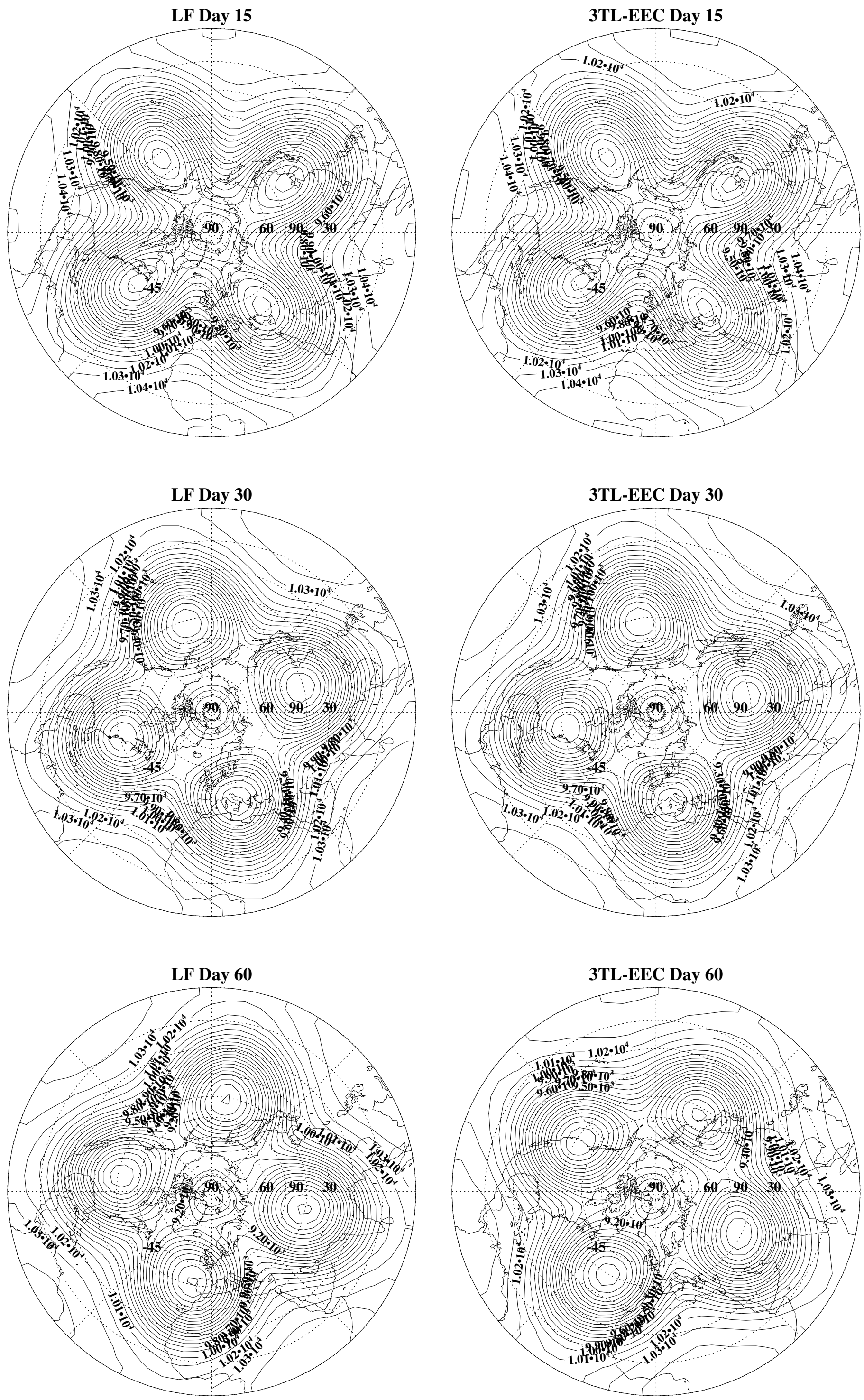

Fig. 5. Same as Fig.4, but the polar filter has been used for the time-filtered LF and 3TL-EEC+LF schemes. The time steps used by the LF and 3TL-EEC scheme are 240 s and 480 s, respectively.

Using the model predicted wind components and height field, we have also computed the global area-averaged total mass (M), total energy (E), and total potential enstrophy (Π), for the entire duration of the time integration. Figure 6 shows the normalized variation of M, E, and Π in time for the time-filtered 3TL-EEC+LF scheme compared to the time-filtered LF scheme. Both schemes display reasonably accurate conservation of the global invariant quantities during the 210 days of time integration. While acceptable level of conservation of M, E, and Π are maintained by both schemes, the polar-filtered LF scheme seems to have an edge over the polar-filtered 3TL-EEC+LF scheme for the conservation of E and Π. Beyond 60 days, the R-H wavenumber 4 pattern starts to unravel that eventually leads to a wavenumber one pattern. For about 50 days, the total potential enstrophy for each scheme remains practically uniform (with and without the polar filter), but gradually dampens after that; whether this is related to the progressive degeneration of the R-H wavenumber 4 into a wavenumber 1 pattern is not necessarily clear.

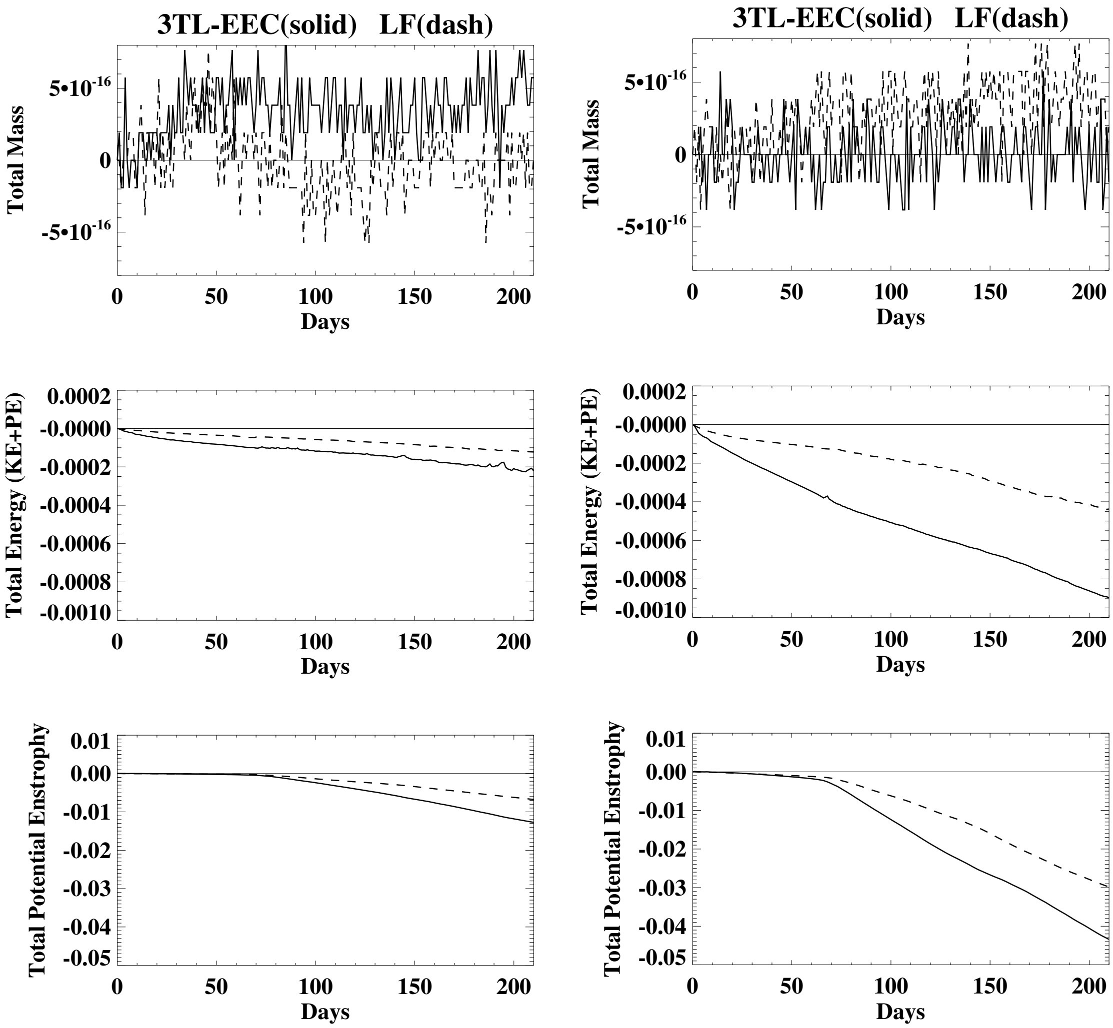

Fig. 6. Time variation of the normalized global integrals of (a) mass, (b), total energy, and (c) potential enstrophy, computed from the forecasts of the global shallow-water model starting with the initial condition shown in Fig. 3. The solid (dashed) curves correspond to the forecasts made using the time-filtered 3TL-EEC+LF (LF) scheme. The 3 panels on the left column correspond to the time integrations without the polar filter, and the 3 panels on the right correspond to the time integrations with the polar filter.

3. Summary

A new three-time-level explicit economical scheme (acronym 3TL-EEC) has been proposed that allows a stable time step for the gravity-wave propagation that is twice as large as the stable time step required by the standard three-time-level leapfrog (LF) scheme. The proposed scheme employs an innovative averaging of the two-time-level forward-backward scheme applied over each of the two time intervals, namely, n-1 to n, and then n to n+1, of the standard leapfrog scheme.

Stability analysis of the LF, 3TL-EEC and 3TL-EEC+LF scheme were performed in context of the 1D and 2D shallow-water gravity waves in presence of advection and rotation. The 3TL-EEC+LF scheme was implemented in a global, grid-point, shallow-water model that conserves mass, total energy, and potential enstrophy in the time continuous case. The shallow-water model was integrated in time for 210 days using the Rossby-Haurwitz zonal wavenumber 4 initial condition. Numerical results were presented for the time-filtered LF and the 3TL-EEC+LF schemes to establish the numerical efficiency, stability, and accuracy of the proposed scheme compared to the LF scheme.

REFERENCES

Arakawa, A., and V. R. Lamb, 1981: A potential enstrophy and energy conserving scheme for the shallow water equations. *Mon. Wea. Rev*. **109**, 18-36.

Asselin, R., 1972: Frequency filter for time integrations. *Mon. Wea. Rev*., **100**, 487-490.

Janjic, Z. I., 2010: Recent advances in global nonhydrostatic modeling at NCEP. *Proceedings of the ECMWF Workshop on Non-hydrostatic Modeling*, Reading, pp. 95-107. ECMWF.

Kar, S. K., R. P. Turco, C. R. Mechoso, and A. Arakawa, 1994: A locally one-dimensional semi-implicit scheme for global gridpoint shallow-water models. . *Mon. Wea. Rev*., **122**, 205-222.

Phillips, N. A., 1959: Numerical integration of the primitive equations on the hemisphere. *Mon. Wea. Rev*., **87**, 333-345.

Robert, A. J., 1966: The integration of a low-order spectral form of the primitive meteorological equations. *J. Meteor. Soc. Japan*, **44**, 237-244.

Williamson, D. L., J. B. Drake, J. J. Hack, R. Jakob, and P. N. Swarztrauber, 1992: A standard test set for numerical approximations to the shallow water equations in spherical geometry. *J. Comput. Phys*., **102**, 211-224.